Article

JOURNAL OF COMPOSITE MATERIALS

Journal of Composite Materials
0(0) 1–14

DOI: 10.1177/0021998310381541
jcm.sagepub.com

SAGE

PLA/clay/wood nanocomposites: nanoclay effects on mechanical and thermal properties

Q.K. Meng, M. Hetzer and D. De Kee

Abstract

Poly(lactic acid) (PLA)/clay/wood nanocomposites were prepared by melt extrusion of PLA, nanoclay, and wood flour (WF). The clay particles exhibit an intercalated structure in the PLA matrix and the addition of WF slightly increases the spacing in the galleries of the intercalated structure. The intercalated clay particles and WF in the PLA matrix restrict the motion of the PLA molecules and crystals. The tensile and flexural moduli of PLA/clay/wood nanocomposites with 30 wt% WF, respectively, increase from 3.75 to 7.08 GPa and from 3.83 to 6.01 GPa compared to neat PLA by adding up to 5 wt% nanoclay. Voids around clay particles, observed via scanning electron microscopy are associated with the negative effect of the clay particles on the interfacial adhesion between the WF and the PLA matrix. Clay particles improve the thermal decomposition temperature (T_d) of PLA/clay/wood nanocomposites by about 10°C compared to that of PLA/wood composites. The effects of clay particles on other thermal properties such as glass transition temperature (T_g), melting temperature (T_m), and linear thermal expansion are also discussed in this article.

Keywords

poly(lactic acid), nanoclay, wood, nanocomposite, material properties

Introduction

Based on their useful properties as well as on sustainability arguments, biopolymers provide alternative options in the category of widely used polymers. Petroleum is the main source for conventional polymers such as polyethylene (PE), polypropylene (PP), poly (vinyl chloride) (PVC), and polystyrene (PS). Although the reserves of crude oil are increasing with the development of new exploration technologies, these reserves are limited. In contrast, the source of biopolymers is renewable and unlimited. Moreover, the conventional widely used polymers are almost nondegradable under normal environmental conditions. Biopolymers deserve earnest consideration and among the biopolymers, poly(lactic acid) (PLA) is intensively being studied.[1–8] Currently, PLA is not so widely used due to some drawbacks of its properties and its high cost. Many approaches are being considered, focusing on improving properties as well as reducing cost. Producing PLA-based composites has proven to be an effective approach to achieve desired properties.[8–17] PLA/wood flour (WF) composites along with PLA/clay nanocomposites have been prepared and characterized by several researchers, achieving improvements in tensile and flexural strengths and muduli,[9,18] storage modulus,[15] heat deflection temperature (HDT),[9] and thermal stability.[18]

WF has been used as reinforcement material in plastics for a long time. WF is a low-density renewable material which offers relative high strength and low abrasion to processing machines.[19] Different types of WF result in different properties of the resulting PLA/WF composites.[9,15] Usually, the addition of 20–50 wt% WF increases tensile and flexural moduli, HDT, and glass transition temperature (T_g). The tensile and flexural strengths of PLA/WF composites are function of the type of WF. Huda et al.[9] used maple WF and their study showed higher flexural strength for PLA/WF composites (118.3 MPa at 20 wt% WF) than 98.8 MPa for pure PLA. However, with increasing WF content from

Department of Chemical and Biomolecular Engineering, Tulane Institute for Macromolecular Engineering and Science, Tulane University, New Orleans, LA 70118, USA.

Corresponding author:
D. De Kee, Department of Chemical and Biomolecular Engineering, Tulane Institute for Macromolecular Engineering and Science, Tulane University, New Orleans, LA 70118, USA
Email: ddekee@tulane.edu

20 to 40 wt%, the flexural strength decreases from 118.3 ± 2.1 to 114.3 ± 5.6 MPa. Note that the magnitudes of the error bars they reported do not justify their conclusion. They reported PLA/WF composite tensile strengths similar to that of pure PLA. The tensile strength decreased from 65.7 ± 1.3 to 58.7 ± 3.1 MPa with increasing WF content from 20 to 40 wt%. The addition of WF decreases the notched Izod impact strength and thermal decomposition temperature compared to the 25.7 ± 1.3 J/m and 385°C (25% weight loss temperature) of pure PLA by ~15% and ~9%, respectively. The interfacial adhesion between the PLA matrix and the WF surface was considered to be the most important factor determining most properties of the PLA/WF composites. Several methods were used to improve the matrix–filler interfacial adhesion, including using maleated polypropylene (MAPP) as compatibilizer, using silane to treat the WF, and using PLA-acrylic acid (PLA-AA) blends as the matrix.[20] These methods improved properties such as tensile strength (~50% increase with PLA-AA matrix from 28 MPa for PLA/30 wt% WF composites), and HDT (69.0°C for PLA/30 wt% WF/5 wt% MAPP composites vs. 66.1°C for PLA/30 wt% WF composites), while impairing others such as storage modulus (8.4 GPa for PLA/30 wt% WF/5 wt% MAPP composites vs. 9.2 GPa for PLA/30 wt% WF composites at 60°C), flexural strength (75.3 MPa for PLA/30 wt% WF/5 wt% MAPP composites vs. 116.6 MPa PLA/30 wt% WF composites), and melting temperature (T_m) (158.1°C for PLA/40 wt% WF/0.5 wt% silane composites vs. 169.1°C for PLA/40 wt% WF composites). Clay is used as a more recent reinforcement filler for polymeric materials. PLA/clay nanocomposites were first prepared by Ogata et al.[21] in 1997 via polymer solution infiltration. Research on PLA/clay nanocomposites soon became popular. Clay addition can substantially improve the properties of PLA-based composites due to its layered structure and nanoscale size. Fully exfoliated clay nanocomposites have a 4.5 GPa storage modulus at 40°C; that of pure PLA at 40°C is 2.8 GPa.[22] More recently, direct melt intercalation/exfoliation has become the standard technique for preparing PLA/clay nanocomposites.[8,23–31] Direct melt intercalated/exfoliated PLA/clay nanocomposites present a tensile strength of 64 MPa improved by ~5%, the flexural strength of 86 MPa improved by ~56%, the O_2 gas permeability coefficient of 200 reduced to 68 mL mm/m^2 day MPa, and the HDT of 76°C improved to 93.2°C with less than 5 wt% clay.

In this contribution we report our research, focusing on PLA-based composites reinforced by both WF and nanoclay. A follow-up article will address the effects of compatibilizers (MAPE, MAPP, and MAPLA) on the mechanical and thermal properties of PLA/clay/wood nanocomposites. Melt extrusion, a continuous manufacturing process widely used in large-scale production, was used to mix the PLA and the fillers. As far as we know, this is the first article on PLA-based composites reinforced by both WF and nanoclay prepared via melt extrusion with a WF content of at least 30 wt%. The only other study dealing with PLA/clay/wood composites reported by Ludvik et al.,[32] involved a low 11 wt% wood loading. Note that economic viability requires an as large as possible wood content. The resulting structure and composite properties are associated with the difference in the sizes of the fillers (~200 μm for WF and ~200 nm for clay). Morphological, mechanical, and thermal properties of PLA/clay/wood nanocomposites are reported in this article. The nanoclay dispersion in a PLA matrix was examined by X-ray diffraction (XRD) and transmission electron microscopy (TEM). The effects of various clay loadings on the properties of PLA/clay/wood nanocomposites are emphasized. The WF contents in our study were 30 and 40 wt%. The addition of WF decreases the cost of the PLA product. The addition of clay improves the T_d, linear thermal expansion, and HDT properties of PLA/WF composites.

Experimental

Materials

The PLA used in this study was PLA 2002D purchased from NatureWorks. The density and melt index of the PLA are 1.24 g/cm^3 and 4–8 g/10 min at 190°C/2.16 kg, respectively. Prior to use, the PLA was dried at 80°C for at least 4 h in a convection oven in accordance with the manufacturer processing guide. The layered silicate used in this study was Cloisite® 20A from Southern Clay Products Inc. It is a natural montmorrilonite (MMT) modified with a quaternary ammonium salt. The density of the clay is 1.77 g/cm^3 with a mean interlayer spacing of the (0 0 1) plane $d_{001} = 24.2$ Å. The clay was dried alongside the PLA. The hardwood (maple) was obtained from ExxonMobil and dried in a convection oven at 90°C to 100°C for at least 24 h prior to use.

Nanocomposite fabrication

All PLA/clay/wood nanocomposite samples were prepared via twin-screw extrusion. A ThermoHaake Rheomex PTW 16/25 twin-screw extruder with screw length (L) of 400 mm was used in this study. The twin-screw extruder had three mixing zones, five temperature zones and a rod die with a diameter of 3 mm. The screw speed was held constant at 150 rpm, and the temperatures were held at 170°C, 180°C, 190°C, 180°C, and 180°C from hopper to die. The feeding rate was adjusted manually to around 25 g/min in order to

maintain the screw torque between 60 and 80 N m. Two processing methods were used to compound PLA with clay and WF: a one-step method and a two-step method. The one-step method is to compound virgin PLA, nanoclay and WF together in a single extrusion process. PLA pellets, nanoclay and WF were manually mixed prior to extrusion. The PLA/clay/wood extrudate was air quenched and pelletized. PLA/clay/wood nanocomposite pellets were then transferred to a convection oven and dried for 24 h at 80°C. In the two-step method, PLA/clay matrices were prepared first by compounding virgin PLA with nanoclay. PLA pellets and nanoclay were manually mixed prior to extrusion. The PLA/clay extrudate was air quenched and pelletized. The prepared PLA/clay matrices were dried in a convection oven at 80°C for 24 h. Next, a certain amount of WF was first manually mixed with PLA/clay matrices and then extruded via twin-screw extrusion. The PLA/clay/wood extrudate was again air quenched and pelletized. The prepared PLA/clay/wood nanocomposites were dried in a convection oven at 80°C for 24 h prior to injection. An alternative compounding order that first produces a PLA/wood matrix, followed by clay addition was also conducted via the two-step method.

A Boy Machines 22A injection molding machine was used to prepare plate and dog-bone test samples. The injection molding machine is composed of a single screw extruder and a mold. The temperature zones were held constant at 165°C, 170°C, 170°C, 175°C, and 180°C from hopper to die. The mold temperature was held constant at 20°C. The plate samples had the following dimensions: $82 \times 60 \times 3\,mm^3$. The dog-bone samples for tensile tests were injection molded using an ASTM D638 type I mold. The flexural test and dynamic mechanical analysis (DMA) samples were die cut to a rectangular shape of $55 \times 13 \times 3$ mm. The thermal mechanical analysis (TMA) samples were die cut to a 12.7 mm diameter.

Characterization methods

A Siemens D500 X-ray diffractometer was used to measure the *d*-spacing of the clay as-received and in the nanocomposites at room temperature. The X-ray beam was Cu-Kα ($\lambda = 0.1540$ nm) radiation, operated at 43 kV and 38 mA. The scanning rate was 0.01°/s and the 2θ ranged from 1.06° to 30°.

A Jeol 2010 TEM was used to examine the nanocomposite morphology at an acceleration voltage 200 kV. The fracture surfaces of the composites after tensile testing were examined using a Jeol JSM-820 scanning electron microscope (SEM) at an acceleration voltage of 20 kV. The samples were sputter-coated with gold prior to observation.

The tensile and flexural tests were performed with an Instron 5582 materials testing machine. The tension tests were based on the ASTM D638 standard at a crosshead speed of 5 mm/min. The flexural tests were based on the ASTM standard D790, involving a three-point bend test at a crosshead speed of 5 mm/min. The testing temperature was 23 ± 1°C according to the ASTM standard. The un-notched Izod impact strength was measured with a Satec BLI impact tester according to ASTM D256.

The TA Instruments DMA 2980 was used to determine HDT using a three-point bending fixture under controlled force mode. The heating rate was 2°C/min. The applied stress was 0.455 MPa. The HDT was defined as the temperature corresponding to a 0.2% strain or a 0.566 mm deflection.

A TA Instruments DSC Q200 was employed to determine the phase transition temperatures (glass transition temperature T_g, melting temperature T_m). The measurement was performed from 20°C to 250°C at a heating rate of 5°C/min under modulated mode. The T_g is defined as the onset temperature of the first steep heat flow decrease; T_m is the melting peak temperature.

The thermal decomposition temperature (T_d) was measured by a TA Instruments TGA 2950 Thermogravimetric Analyzer from 25°C to 580°C at a heating rate of 10°C/min with nitrogen as purge and balance gas. The onset temperature of steep weight decrease was used as T_d.

The linear thermal expansion coefficient (α) was measured via a TA Instruments TMA 2940 Thermomechanical Analyzer from room temperature at a heating rate of 2.00°C/min up to 90°C with 0.050N applied force.

Results and discussion

Determination of processing procedure

At constant extrusion temperatures, screw speed and feeding rate, two processing methods that refer to one-step and two-step methods as described earlier were conducted for PLA/clay/wood nanocomposite with 3 wt% nanoclay and 30 wt% WF. Under the two-step method, two compounding procedures for PLA/clay/wood mixing were tested to select an effective and convenient compounding route to extrude PLA/clay/wood nanocomposites. The mechanical and thermal properties of the samples were compared to determine which method or compounding procedure would be used for the further research. The experimental data and fabrication feasibility indicated that the two-step method mixing a PLA/clay matrix first would be the best choice to achieve better properties and fabrication convenience.

Table 1. Comparison of mechanical and thermal properties of PLA-based nanocomposites with 3 wt% nanoclay and 30 wt% WF fabricated by three different compounding processes (one-step method, two-step method of first making PLA/clay matrix, and two-step method of first making PLA/wood matrix)

Properties	P3C30W-one-step	P3C30W-two-step	P30W3C-two-step
Tensile modulus (GPa)	7.15 ± 0.61	6.65 ± 0.27	7.06 ± 0.27
Tensile strength (MPa)	40.38 ± 0.63	48.03 ± 0.48	44.26 ± 0.68
Strain at maximum tensile stress (%)	1.15 ± 0.05	1.33 ± 0.02	1.16 ± 0.04
Flexural modulus (GPa)	5.16 ± 0.18	5.40 ± 0.17	5.64 ± 0.31
Flexural strength (MPa)	65.19 ± 1.78	67.07 ± 1.13	68.26 ± 1.25
T_d (°C)	395.75	398.71	391.98
HDT (°C)	58.22 ± 0.23	59.27 ± 0.24	58.82 ± 0.30
d_{001} (nm)	3.42	3.53	3.40

Some mechanical and thermal properties of three samples (P3C30W-one-step, P3C30W-two-step, and P30W3C-two-step) are compared in Table 1. Here, P3C30W-one-step refers to the one-step method sample with 3 wt% nanoclay and 30 wt% WF; P3C30W-two-step refers to the two-step method that involves preparing PLA/clay matrix first and then adding WF; and P30W3C is the sample prepared by the other two-step method compounding procedure. Taking error bars into account, one concludes that these three samples have similar tensile and flexural moduli and strength. Although the P3C30W-one-step sample has the highest average tensile modulus (7.15 GPa), the one-step method results in a ~15% decrease in tensile strength and in strain at maximum tensile stress relative to the values (48.03 MPa and 1.33%) of the P3C30W-two-step sample. The P30W3C-two-step sample also shows decreased tensile strength and strain compared to the P3C30W-two-step sample. The XRD patterns reveal similar intercalated clay structures for these three samples. Their interlayer spacings (d_{001}) are 3.42, 3.53, and 3.40 nm as shown in Table 1. These three compounding processes all lead to intercalated clay structure in the nanocomposites, but due to different extrusion times involving nanoclay (twice for P3C30W-two-step, and once for the other two samples) the dispersion of intercalated clay particles in the nanocomposites is different case by case. The two-time extrusion of nanoclay should contribute to a more uniform dispersion of the intercalated nanoclay particles in the polymer matrix. The high tensile strength associated with the P3C30W-two-step can be attributed to the uniform dispersion of the intercalated nanoclay particles. Furthermore, the uniform dispersion of the intercalated nanoclay particles slightly decreases the brittleness of the nanocomposites as observed from the data of strain at maximum tensile stress. The wetting of WF is also affected by the compounding process. That is to say: the one-step method results in lesser WF wetting due to the increased probability of nanoclay particles attaching to the WF surface. This reduced WF wetting also leads to a decrease in tensile strength, thermal decomposition and HDT. Note that the P3C30W-two-step sample in Table 1 has the highest thermal decomposition and HDTs as a result of enhanced clay particle dispersion and WF wetting. A comparison of the mechanical and thermal properties leads to the choice of the two-step method with the compounding order involving PLA/clay matrix preparation, followed by wood addition, for further study. In the following sections, abbreviations, such as P0C30W and P3C30W, all refer to two-step method samples whose compounding order entails making a PLA/clay matrix first, followed by WF addition.

XRD patterns and TEM images

The structure of the dispersed silicate layers in nanocomposites determines the reinforcement efficiency of nanoclay in terms of the extent of nanoclay dispersion/exfoliation. XRD (via diffraction angles, peak intensity, and peak shape), is an acknowledged tool to analyze the nanostructure of dispersed silicate layers in nanocomposites. TEM is another widely used tool to visually observe the nanostructure. These two complementary types of characterization are used concurrently. Figure 1 shows XRD patterns for nanoclay as well as for PLA/clay matrices with clay loadings of 1–5 wt%. The 2θ angle corresponding to the diffraction peak of pure clay-Cloisite® 20A is 3.960°, which can be used to calculate the mean d-spacing between two single silicate layers. This spacing is 2.23 nm for pure clay which is oven dried at 90°C for 24 h. This result is lower than the value of 2.42 nm that is given by the clay manufacturer. This is due to the water trace absorbed in nanoclay which enhances the hydrogen bonds between silicate layers. The 2θ angles are 2.539, 2.500, and 2.504° for the 1, 3, and 5 wt% clay cases, respectively. The corresponding mean d-spacing values

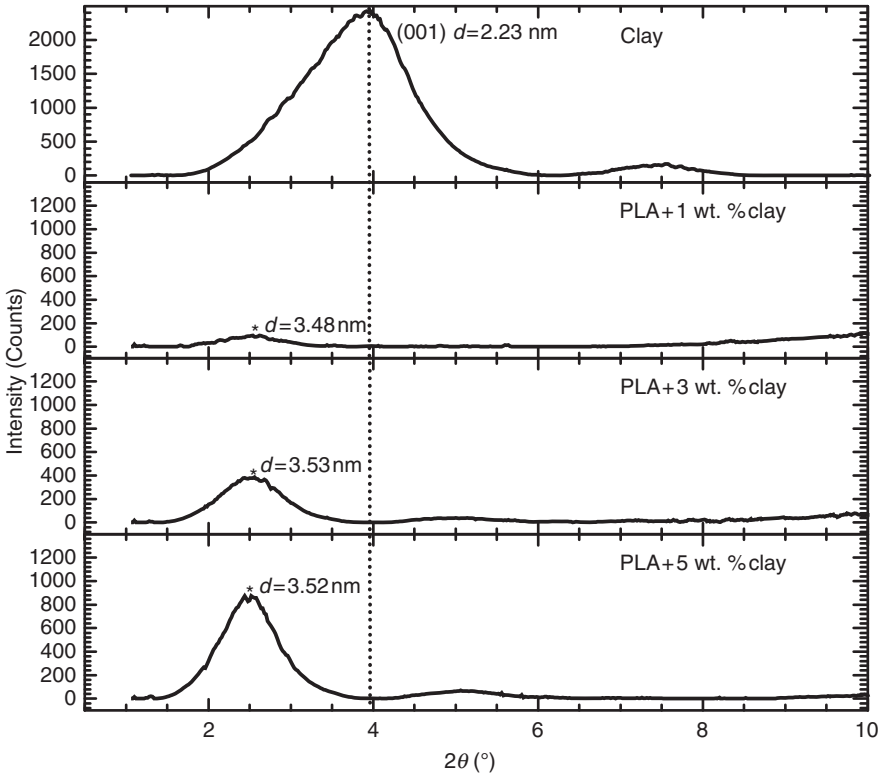

Figure 1. XRD patterns of nanoclay (Cloisite® 20A) and PLA/clay nanocomposites with clay loadings of 1, 3, and 5 wt%.
Note: The dotted line identifies the position of the nanoclay (0 0 1) diffraction peak; the stars indicate the positions of the nanoclay diffraction peaks.

are 3.48, 3.53, and 3.52 nm. The mean *d*-spacing is due to the infiltration of PLA chains into the silicate layer galleries. The results indicate that 3 wt% clay seems to be the optimum value for clay loading. The XRD intensity is associated with the fraction of ordered silicate layers in the PLA matrix. The diffraction peak intensity increases up to 875 counts as the clay loading increases from 1 to 5 wt%. The nanoclay intercalated structure in the PLA matrix displays an increased *d*-spacing, and several single silicate layers still stack together forming micro-size particles. There is another peak at 7.450° in the case of pure clay. It should belong to the (0 0 1) diffraction peak of sepiolite which is a clay mineral component. Serna et al.[33] reported that the first sharp diffraction peak of sepiolite appeared at 12.1 Å. Sepiolite has a structure similar to the tetrahedral–octahedral–tetrahedral sandwich crystal structure of montmorillonite. Base on the $d_{001} = 2.23$ nm, one can calculate the (0 0 2) plane diffraction angle for montmorillonite as $2\theta = 7.925°$. This 2θ value is higher than 7.450° for the sepiolite. The diffraction peak of the sepiolite in the clay possibly masks the (0 0 2) diffraction peak. The small second diffraction peaks of the PLA/clay nanocomposite patterns are likely associated with PLA infiltration of sepiolite galleries. One determines the diffraction angle of the (0 0 2) plane ($2\theta = 7.925°$) via Bragg's law with $\lambda = 1.541$ Å, $d\,[= d(0\,0\,1)] = 2.23$ nm, and $n = 2$.

Figure 2 illustrates the XRD patterns of PLA/clay/wood nanocomposites with clay loadings of 1–5 wt%. The wood content of these nanocomposites is 30 wt% based on the total composite weight. The *d*-spacing values of the nanoclay in the PLA/clay/wood nanocomposites are 3.59, 3.53, and 3.44 nm as the clay loading increases from 1 to 5 wt%. Note that these values are higher than that of pure clay (2.23 nm). Intercalated nanoclay is also the dominant structure in the PLA/clay/wood nanocomposites. Compared to those PLA/clay matrices, the *d*-spacing value in P1C30W is larger than that in the corresponding PLA/clay matrix (P1C). Here, 1C refers to 1 wt% clay and 30W refers to 30 wt% WF. The second extrusion process which extruded the PLA/clay matrix with WF promotes further infiltration of PLA chains. The WF added in the second extrusion process likely increases the shear stress applied on the clay particles, resulting in improved intercalation, while P5C30W has a lower *d*-spacing than P5C. A clay loading (>3 wt%) makes the nanoclay particles in a PLA matrix aggregate upon addition of WF. Although the decrease of *d*-spacing is very small ($\sim 10^{-2}$ nm), the result indicates that a 3 wt% clay loading allows for an optimum dispersion/PLA

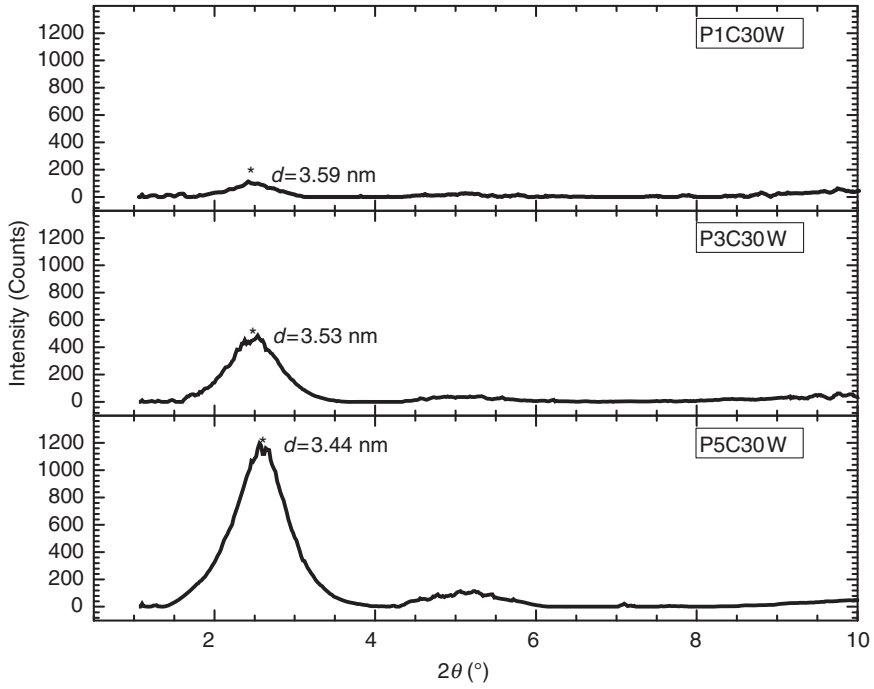

Figure 2. XRD patterns of PLA/clay/wood nanocomposites with 30 wt% wood content and clay loadings of 1, 3, and 5 wt%, respectively.
Note: The stars identify the position of the nanoclay diffraction peaks.

chain infiltration. A clay loading below 3 wt% is preferable for clay dispersion/intercalation. The second diffraction peaks are also due to the presence of intercalated sepiolite. The clay in either PLA/clay matrices or PLA/clay/wood nanocomposites is intercalated and the intercalated structure is not significantly affected by the WF. Because of the large size difference between WF and nanoclay particles and the small nanoclay loading, the effect of clay particles on the dispersion of WF in the PLA matrix is not obvious compared to the study of Ludvik et al.[32] They used more than 8 wt% sodium bentonite clay to uniformly disperse cellulose fiber in the PLA matrix. TEM was used to observe the local dispersion of nanoclay in the PLA matrix.

Figure 3 illustrates the typical bright field images of PLA/clay matrices in which the dark areas identify the cross-section of intercalated and flocculated silicate layers. Clay is oriented parallel to the surface. This depends on the way the sample was sectioned from the bulk material. The clay is fairly well dispersed; however, some aggregates can be observed in the 1 wt% clay case (Figure 3(a)). It appears that the clay dispersion and the size of the intercalated and flocculated clay particles are slightly more uniform in the 3 wt% clay sample (Figure 3(b)). There are some aggregates present in this sample also, but those are less common than in the 1 wt% clay sample. Also, the protuberances are not as large as in the 1 wt% clay sample. A single silicate layer has a thickness of ~1 nm and an average length of ~100 nm. The length of the stacked intercalated silicate layers appears to be about 300–500 nm (Figure 3(a)). This is due to the hydroxylated edge–edge interaction of the silicate layers that promote silicate layer flocculation. Figure 3(b) allows for the observation that the silicate layers appear to align in the preferred melt flow direction as indicated by the arrow. The injection-molded samples reveal the clay melt flow direction alignment.

Morphology of the fracture surface

The fracture surfaces of the composites used in tensile tests were observed by SEM. Figure 4 shows the morphology of a fracture surface of a PLA/30 wt% wood composite at different amplification scales. In Figure 4(a), the fracture surface of large WF (length > 200 μm) was observed as shown by arrow 1. It is common for large WF particles, whose fiber alignment direction is normal to the tension force direction, to break along the fracture surface indicating improved WF-PLA matrix interfacial adhesion. The strength of the adhesion between parallel cellulose fibers should be less than the ultimate tensile strength of the PLA matrix. Smaller WF particles (length < 200 μm) as well as large WF particles whose fiber alignment is parallel to the external tension direction were mostly pulled out from the PLA matrix. This left protruded WF and dents on the fracture surface as identified by arrows

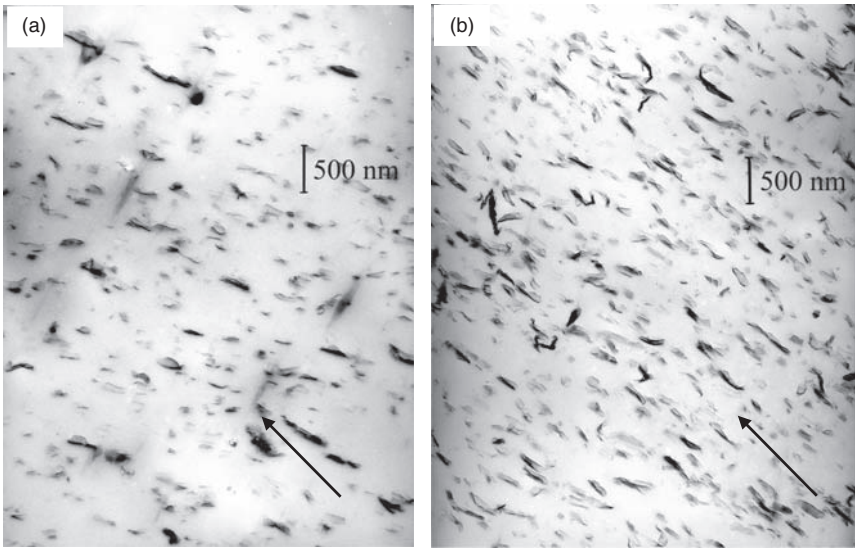

Figure 3. TEM bright field images of PLA/clay matrices: (a) 1 wt% clay; and (b) 3 wt% clay.
Notes: The dark spots identify the cross-section of intercalated clay particles, and the bright areas refer to PLA. The arrow refers to the melt flow direction.

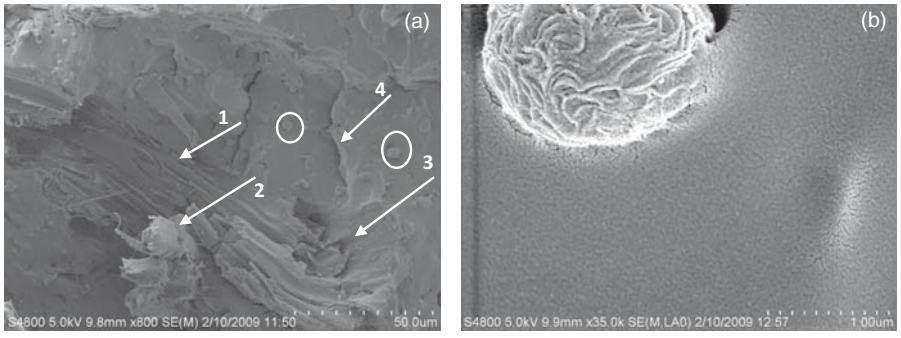

Figure 4. SEM images of the fracture surface of PLA/30 wt% wood composite: (a) 50.0 μm; and (b) 1.00 μm.

2 and 3. Some cracks (arrow 4) in the PLA matrix were also observed. Micro-size balls, (Figure 4(b)), are small wood fibers encapsulated by the polymer matrix. The rough surface of the WF particles could benefit the interfacial adhesion between the WF and the PLA matrix. The PLA matrix in Figure 4(b) shows a smooth surface; no small particles are observed. The WF in the PLA matrix displays good interfacial adhesion, but because of the various sizes and shapes of WF particles, interfacial adhesion deficiencies always exist, which to a certain extent weaken the reinforcement effect of WF. Generally speaking, the reinforcement effect of WF is mainly determined by the interfacial adhesion between the WF and the PLA matrix as well as the dispersion of WF particles.

Figure 5 shows tensile test fracture surfaces of PLA/clay/wood nanocomposites with various clay loadings. In Figure 5(a), some spots (~100 nm) were observed which were believed to be intercalated and flocculated clay particles. Note the contrast with the smooth surface in Figure 4(b). As the clay loading was increased to 5 wt%, the spots shown on the surface increased (Figure 5(b) and (c)). Note that the clay particles appeared to be partially raised, forming dents on the surface. The clay particles that protrude from the surface tend to reduce the system tensile strength. The data in Figure 6 support this statement. The XRD and TEM data/images indicated that the clay particles were compounded in the PLA matrix mostly in the form of intercalated and flocculated structures with interlayer spaces that create voids under an applied tension force. Figure 5 confirms the voids around the nanoclay particles and more and larger voids appear when the nanoclay loading increases to 5 wt%. Furthermore, the clay particles attached on WF surfaces reduce the interfacial adhesion between the WF and the PLA matrix. The adhesion strength between WF and nanoclay particles is less than that between the WF and the PLA matrix.

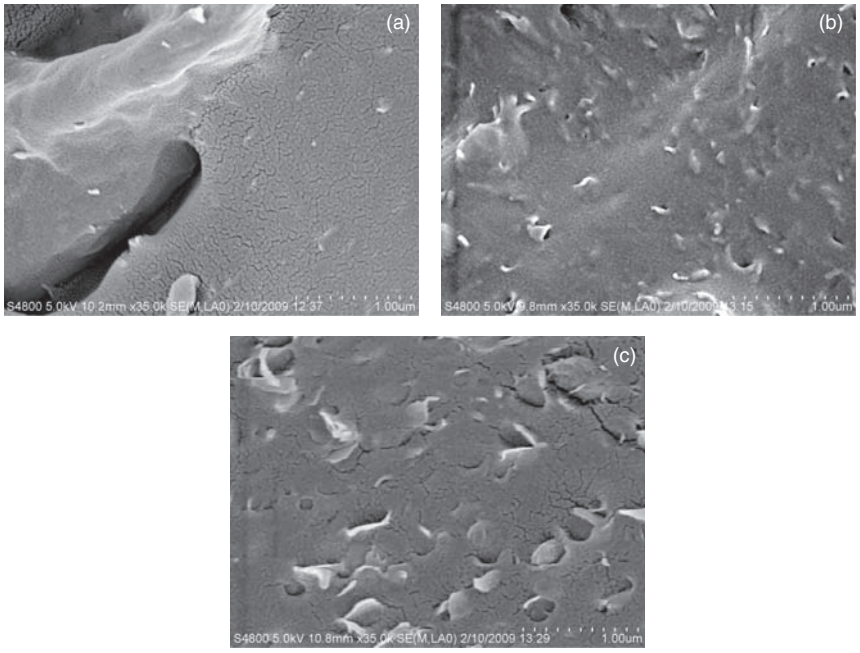

Figure 5. SEM images of fracture surfaces of PLA/clay/30 wt% wood nanocomposites with clay loadings of 1–5 wt%: (a) P1C30W; (b) P3C30W; and (c) P5C30W.

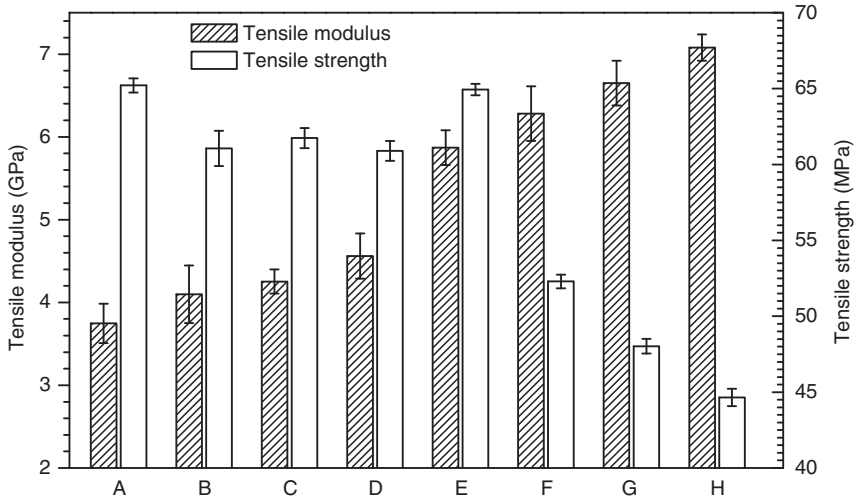

Figure 6. Tensile properties of PLA, PLA/clay matrices and PLA/clay/wood nanocomposites: (A)–(H) represent pure PLA, P1C, P3C, P5C, P0C30W, P1C30W, P3C30W, and P5C30W, respectively.

Mechanical properties

The mechanical properties we discuss here include Young's modulus, ultimate tensile strength, flexural modulus, flexural strength, and un-notched Izod impact strength. The mechanical properties of the control PLA are compared to those of the composites with 30 wt% WF and various clay loadings, in Table 2. Except for its brittleness, pure PLA has excellent mechanical properties compared to some conventional polymers such as PE, PP, etc.

Table 2 indicates that the tensile modulus increases significantly with the addition of 30 wt% WF, while the tensile strength remains nearly the same as that of pure PLA. This implies that the WF incorporated in the PLA matrix has wetting properties that result in effective reinforcement. When the WF content was increased to 40 wt% (not shown in Table 2), the tensile

Table 2. Mechanical properties of pure PLA and PLA/clay/wood nanocomposites with 1, 3, and 5 wt% clay, respectively

	Mechanical properties				
Sample	Tensile modulus (GPa)	Tensile strength (MPa)	Flexural modulus (GPa)	Flexural strength (MPa)	Impact test value (J/m)
Pure PLA	3.75 ± 0.24	65.21 ± 0.47	3.83 ± 0.07	104.02 ± 0.78	238.2 ± 33.0
P0C30W	5.87 ± 0.21	64.94 ± 0.38	4.88 ± 0.02	88.11 ± 2.93	164.2 ± 14.4
P1C30W	6.28 ± 0.33	52.29 ± 0.45	5.06 ± 0.06	78.64 ± 0.59	159.8 ± 22.1
P3C30W	6.65 ± 0.27	48.03 ± 0.48	5.40 ± 0.17	67.07 ± 1.13	137.7 ± 9.6
P5C30W	7.08 ± 0.16	44.65 ± 0.57	6.01 ± 0.22	66.53 ± 3.43	132.3 ± 22.7

modulus and tensile strength were measured to be 7.05 ± 0.27 GPa and 57.89 ± 0.86 MPa, respectively. Compounding too much WF (>30 wt%) reduces the wetting of WF particles by the PLA matrix and introduces more interfacial adhesion deficiencies. This is due to the fact that more wood surface is available within a lesser amount of polymer. Furthermore, WF is anisotropic and the strength in the longitudinal direction is about 40 times higher than that in the direction perpendicular to the grain.[34–36] That is: the strength of WF is sensitive to the orientation of the WF relative to the direction of the applied load. A grain angle of 15° relative to the direction of the applied tension reduces the tensile strength by almost 60% of the value when the tension is axial. The alignment of WF particles in the PLA matrix is random, and this reduces the reinforcement capacity of the WF. The addition of nanoclay increases the tensile modulus further, and the Young's modulus of P5C30W is almost twice that of pure PLA. The tensile strength starts to decrease with increasing clay loading. By adding clay up to 5 wt%, the tensile strength decreases by about 20 MPa in contrast to that of P0C30W. The tensile modulus increase is mainly determined by the WF and nanoclay particle configuration that restricts the motion of the polymer molecules. Note that the WF and clay particles exhibit large size differences (WF ~200 μm, clay particles ~200 nm). The filler dispersion thwarts, to some extent, the relative motion under external tension, of matter over a range incorporating small polymer chains to larger crystals. The reduced deformability of the polymer matrix also results in a decrease in the elongation at break from 1.94% for pure PLA to 1.06% for P5C30W. The tensile strength is determined by the strength of the polymer matrix and the fillers, and their interfacial adhesion. The tensile properties of pure PLA and PLA/clay matrices are compared in Figure 6. The tensile modulus increases with clay addition. However, the tensile strength of the PLA/clay matrices is somewhat lower than that of pure PLA. Different clay loadings do not result in a significant variation in the tensile strength of these PLA/clay matrices. The intercalated and flocculated nanoclay structure should account for the decrease in the tensile strength because of the voids they introduced.

The interfacial adhesion of PLA/PLA-clay matrices and WF was observed and compared in the SEM images of the tensile breakage surfaces in Figure 7. The circles in Figure 7(a) indicate WF breakage surfaces. Rougher (more uneven) surfaces can be observed in Figure 7(b)–(d), where the arrows identify larger voids and the traces of protruding WF particles. Apparently, the presence of clay particles in the composites reduces the interfacial adhesion between the matrix and the WF. The clay particles on or near the WF particles are likely at the origin of the formation of micro-size voids when tension is applied.

The flexural properties follow a similar trend as that of the tensile properties listed in Table 2. The flexural modulus of PLA/WF composites is about 1 GPa higher than that of pure PLA; roughly a 30% increase. The clay particles in the PLA/clay/wood nanocomposites further increase the flexural modulus up to 6.01 GPa with a clay loading of 5 wt%. The reduced deformability resulting from the configuration of the WF and clay particles is associated with the increase in the flexural modulus. The addition of 30 wt% WF decreases the flexural strength from 104.02 MPa (pure PLA) to 88.11 MPa, which is contrary to the results obtained by Huda et al.,[9] who used different PLA and WF as well as different processing procedures. The addition of clay particles further decreases the flexural strength to 66.53 MPa at a clay loading of 5 wt%. This is also associated with the reduced deformability and wood-PLA interfacial adhesion.

The un-notched Izod impact strength of pure PLA decreases from 238.2 to 164.2 J/m upon addition of 30 wt% WF. The addition of 5 wt% clay particles further decreases the impact strength to 132.3 J/m. The impact strength mainly describes material brittleness. WF and clay particles cannot improve the brittleness of the PLA matrix. The structure created by the WF and clay particle dispersion renders the PLA matrix more brittle (Table 2).

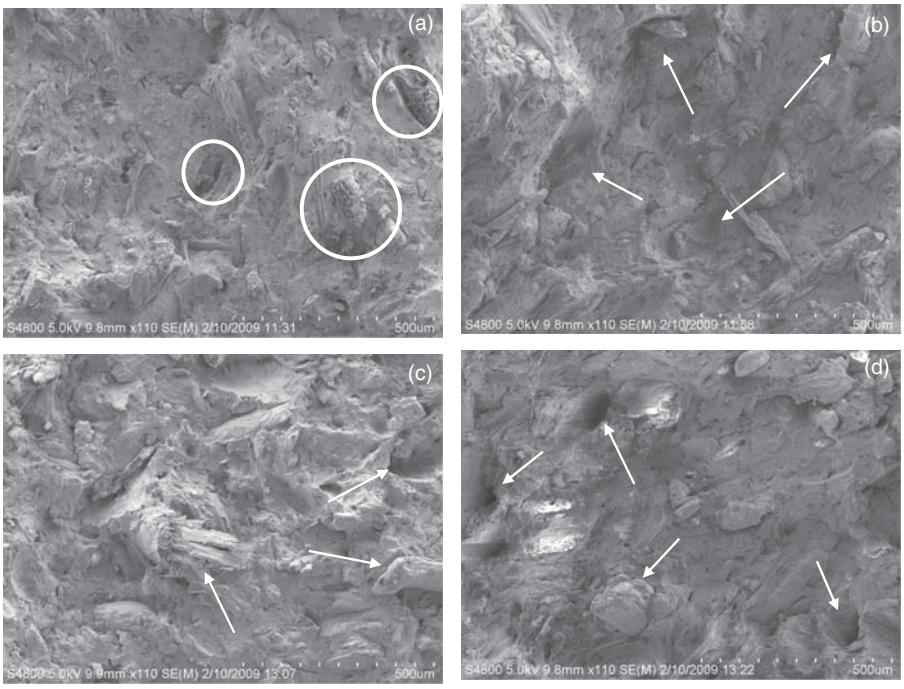

Figure 7. SEM images of PLA/clay/wood nanocomposites: (a) no clay; (b) 1 wt% clay; (c) 3 wt% clay; and (d) 5 wt% clay.

Thermal properties

Figure 8 shows thermogravimetric curves for PLA, WF, and composites. The composite material involving only WF has a T_d of 387.6°C; the T_d of pure PLA is 408.8°C. The thermogravimetric curve for WF reveals a T_d of 321.07°C (Table 3) which is much lower than the 408.80°C for pure PLA. The low T_d of WF and the trace of moisture introduced by the WF contribute to the thermal decomposition temperature decrease. The moisture in the composite materials accelerates the pyrolytic process of the PLA matrix.[37] The T_d tends to decrease further with increasing WF loading.[9] The T_d increased by 6.8°C with the addition of 1 wt% clay into the PLA/wood composite material; 3 wt% clay resulted in a further increase of 2.4°C, and there is no further increase as the clay loading was increased to 5 wt%. Clay particles can substantially increase the T_d of PLA/clay/wood nanocomposites compared to that of PLA/wood composites. The intercalated clay particles allow for stabilizing and barrier effects.[38,39] The dispersion structure formed by clay particles restricts the configuration of PLA molecular chains and reduces the probability of the initial oligomers produced by thermal decomposition to activate further decomposition.[40,41] The clay particles also act as a barrier to gas permeation. Although the 3 and 5 wt% clay samples yield similar T_d values, the maximum thermal decomposition rate (Figure 9) decreases and shifts to a slightly higher temperature as the clay loading increases from 3 to 5 wt%. The maximum thermal decomposition rate of pure PLA occurs at ~440°C at a rate of about 2.5%/°C. For WF,

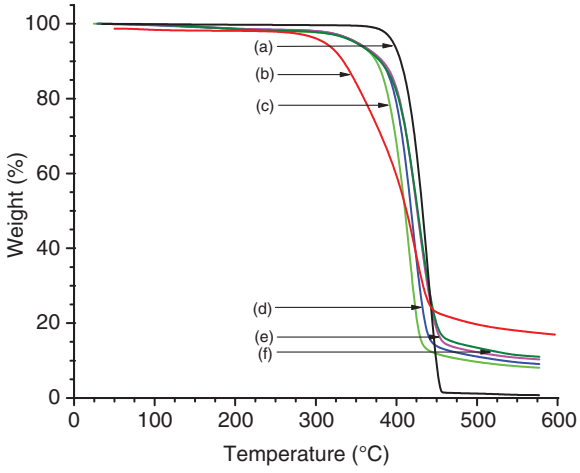

Figure 8. Thermogravimetric curves of PLA, WF, and composites: (a) neat PLA; (b) wood four; (c) P0C30W; (d) P1C30W; (e) P3C30W; and (f) P5C30W.

the equivalent data are ~424%/°C and 1.0%/°C. The P0C30W sample shows an intermediate thermal decomposition peak rate of 2.2%/°C, but the maximum thermal decomposition rate temperature of 399°C is lower than that of WF. This confirms the synergistic effect[42] between the WF and the PLA, which promotes the start of thermal decomposition. With adding clay (1–5 wt%), the maximum thermal decomposition rate temperature of the PLA/clay/wood nanocomposites increases from 420.3 ± 0.4°C to 426.8 ± 0.3°C, and the maximum thermal decomposition rate decreases from 2.0%/°C to

Table 3. Thermal properties of PLA/clay/wood nanocomposites

Thermal properties	PLA	WF	P0C30W	P1C30W	P3C30W	P5C30W
T_d °C	408.8	321.1	387.6	394.4	396.8	396.2
T_g °C	52.3	–	51.7	51.0	51.1	51.5
T_m °C	150.4	–	150.2	150.3	151.2	150.4
χ%[a]	31.7	–	24.0	18.1	17.3	20.1
HDT °C	56.5	–	55.7	56.3	56.0	56.5

[a]Percent crystallinity calculated on the basis that a 100% crystalline PLA has a ΔH value of 93.6 J/g.

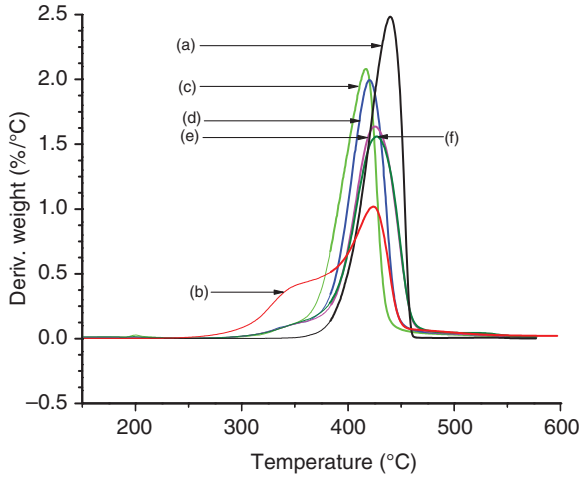

Figure 9. Derivative thermogravimetric curves from Figure 8 of PLA, WF, and composites: (a) neat PLA; (b) WF; (c) P0C30W; (d) P1C30W; (e) P3C30W; and (f) P5C30W.

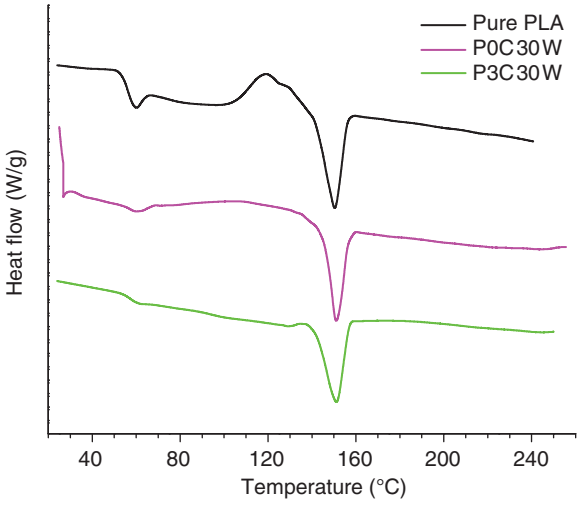

Figure 10. DSC curves of pure PLA, PLA/wood composite, and PLA/wood/clay nanocomposites P3C30W.
Note: The upward direction refers to the exothermic direction.

1.88%/°C, respectively. This confirms that the intercalated clay particles restrict the motion of (oligomer) molecular chains, resulting in a decreased maximum thermal decomposition rate.

Some thermal properties of PLA, WF, and composites are shown in Table 3. The addition of clay does not result in large variations in glass transition temperature (T_g), melting temperature (T_m), and HDT compared to those of pure PLA and PLA/wood composites. Differential scanning calorimetry (DSC) was used to measure the T_g and T_m based on the first heating scan. Figure 10 shows the DSC curves for pure PLA, P0C30W, and P3C30W. The data for pure PLA show an apparent glass transition step, whereas, the glass transition steps of P0C30W and P3C30W appear more flattened. WF and nanoclay may retard the heat diffusion in the composite materials.[39] The DSC curve of P3C30W identifies a slow monotonically decreasing trend, whereas that of P0C30W is associated with a falling and rising trend before the melting point. This is associated with a long-lasting retardation effect that correlates with the clay nano-scale size. The T_g of PLA/wood composites and PLA/clay/wood nanocomposites are slightly less than that of pure PLA. At around 130°C pure PLA shows a crystallization peak which is absent for P0C30W and P3C30W. That is to say, the presence of wood four and nanoclay particles prevent small crystals or long molecular chains from forming large crystals. They all have a similar melting temperature of ~150°C. When the PLA crystals begin to melt and most molecular chains move more freely, the heat retardation effect of the WF and nanoclay becomes negligible.

Huda et al.[9] reported that the addition of 32–40 wt% WF can increase the HDT of pure PLA from 64.5°C to 67.6°C. However, Table 3 shows that the HDT of P0C30W is slightly lower than that of pure PLA. Again, Huda et al.[9] used different PLA and WF. They also applied different loading stresses; that is: we used 0.455 MPa as opposed to 0.46 MPa in Huda et al.'s tests. Poor matrix–filler interfacial adhesion will result in more rapid sample failure under a higher loading stress. Furthermore, the crystallinity decrease from 31.7% to 24% also contributes to the HDT decrease. The nanocomposites have similar HDTs to that of pure PLA.

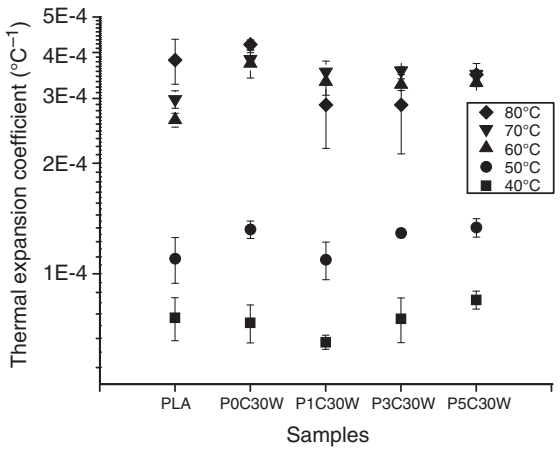

Figure 11. Linear thermal expansion coefficients of PLA and PLA/clay/30 wt% wood nanocomposites with 1, 3, and 5 wt% clay, respectively.

The linear thermal expansion coefficient characterizes the linear dimensional stability of materials. Figure 11 shows the linear thermal expansion coefficients of neat PLA, PLA/wood, and PLA/clay/wood nanocomposites as a function of temperature. In our study, the linear thermal expansion coefficient whose direction is perpendicular to the injection flow direction was measured. The linear thermal expansion coefficient of pure PLA increases from 7.6×10^{-5} to 3.8×10^{-4} μm/°C as the temperature increases from 40°C to 80°C. Because the T_g of pure PLA is around 52°C, there is a 1.52×10^{-4} μm/°C difference between the linear thermal expansion coefficients at 50°C and 60°C. When WF was added, the linear thermal expansion coefficient increased from the value for pure PLA over the temperature range of 50–80°C, but decreased slightly at 40°C. Voids between the PLA matrix and WF particles contribute to the increase. The addition of 1 wt% clay did decrease the linear thermal expansion coefficients of P0C30W at all temperatures, especially at 80°C. Adding 3 or 5 wt% clay particles increases the linear thermal expansion coefficients compared to the 1 wt% clay case below the T_g of pure PLA. Clay particles likely act as lubricant to reduce the interfacial adhesion between the WF and the PLA matrix. Above the T_g of pure PLA, the addition of 3 or 5 wt% nanoclay particles did not increase the linear thermal expansion coefficients of the PLA/clay/wood nanocomposites compared to the 1 wt% nanoclay case except for the case involving a 5 wt% clay loading and a temperature of 80°C. A clay loading of <1 wt% reduces the thermal expansion coefficient of the PLA/wood composites over the temperature range 40–80°C. The structure created by the clay particle dispersion contributes to the decrease of the linear thermal expansion coefficient. However, a clay loading greater than 1 wt% can result in the opposite effect due to a negative effect on the interfacial adhesion between the WF and the PLA matrix (Figure 7).

Conclusions

PLA, a promising biopolymer, is problematic in terms of cost and brittleness. WF is usually added to reduce the cost, meanwhile improving some mechanical and thermal properties of the PLA matrix. We used WF as well as nanoclay to reinforce PLA. As far as we know, this is the first research on melt extrusion prepared PLA-based composites reinforced by both nanoclay and WF with 30 wt% or more WF content. XRD tests showed that the clay particles in PLA/clay/wood nanocomposites adopt an intercalated structure similar to that of PLA/clay nanocomposites. That is: the addition of WF does not affect the dispersion of clay particles in a PLA matrix. Tensile, flexural and impact tests indicated that various clay loadings affect the mechanical properties of PLA/clay/wood nanocomposites. The tensile modulus increases from 3.75 GPa for neat PLA to 7.08 GPa for PLA/clay/wood nanocomposite with a 5 wt% clay loading. However, the tensile strength experienced a decrease of around 20 MPa with the addition of up to 5 wt% clay. The flexural modulus and strength follow a similar trend as the tensile properties. The highest flexural modulus in our study is 6.01 GPa for P5C30W, but its flexural strength decreases to 66.53 MPa compared to 104.02 MPa for neat PLA. The impact strength was not improved upon addition of WF and clay particles. The impact strength decreased from 238.2 J/m for neat PLA to 132.3 J/m for P5C30W. Clay particles result in increased tensile and flexural moduli and in decreased tensile, flexural and impact strengths. The structure created by WF and nanoclay particle dispersion contributes to increases in the moduli and to the decrease in impact strength. The clay particles have an adverse effect on the interfacial adhesion between the WF particles and the PLA matrix. SEM images confirm that the clay particles in the PLA matrix cause voids that weaken the mechanical properties.

The addition of clay particles considerably decreased the thermal decomposition rate and shifted the peak rate to a higher temperature. The filler material hinders the creation of higher crystallinity in the PLA matrix. The melting temperature of PLA/clay/wood nanocomposites was found to be nearly the same as that of neat PLA. Different clay loadings did not change the T_g of PLA/clay/wood nanocomposites. Instead of changing the T_g, the clay particles broadened the glass transition step. A less than 1 wt% clay loading improved the linear dimensional stability of PLA/clay/wood nanocomposites. A clay loading beyond 1 wt% appears to

introduce a more intercalated clay particle structure that acts as an interfacial lubricant.

The interaction between WF and intercalated clay particles, a 'large-small-filler' melt colloid system, will need further study. The improvement in the impact strength should be emphasized in future research.

Acknowledgments

The authors gratefully acknowledge financial support via LEQSF grant RD-B-07 and NASA grant NNX08AP04A. This material was also based on work supported by the National Science Foundation, while DDK was working at the Foundation.

References

1. Andreopoulos AG, Hatzi E and Doxastakis M. Synthesis and properties of poly(lactic acid). *J Mater Sci: Mater Med* 1999; 10: 29–33.
2. Baiardo M, Frisoni G, Scandola M, Rimelen M, Lips D, Ruffieux K, et al. Thermal and mechanical properties of plasticized poly(L-lactic acid). *J Appl Polym Sci* 2003; 90: 1731–1738.
3. Bandyopadhyay S, Chen R and Giannelis EP. Biodegradable organic-inorganic hybrids based on poly(L-lactide). *Polymer* 1999; 81: 159–160.
4. Celli A and Scandola M. Thermal-properties and physical aging of poly(l-lactic acid). *Polymer* 1992; 33: 2699–2703.
5. Chang JH, An YU, Cho D and Giannelis EP. Polylactide nanocomposites: comparison of their properties with montmorillonite and synthetic mica (II). *Polymer* 2003; 44: 3715–3720.
6. De Oca HM and Ward IM. Structure and mechanical properties of poly(L-lactic acid) crystals and fibers. *J Polym Sci Part B-Polym Phys* 2007; 45: 892–902.
7. Feng JT, Sui JH, Cai W and Gao ZY. Microstructure and mechanical properties of carboxylated carbon nanotubes/poly(L-lactic acid) composite. *J Compos Mater* 2008; 42: 1587–1595.
8. Ray SS and Bousmina M. Biodegradable polymers and their layered silicate nanocomposites: in greening the 21st century materials world. *Prog Mater Sci* 2005; 50: 962–1079.
9. Huda MS, Drzal LT, Misra M and Mohanty AK. Wood-fiber-reinforced poly(lactic acid) composites: evaluation of the physicomechanical and morphological properties. *J Appl Polym Sci* 2006; 102: 4856–4869.
10. Lee SH and Wang SQ. Biodegradable polymers/bamboo fiber biocomposite with bio-based coupling agent. *Compos Part A* 2006; 37: 80–91.
11. Lee S-Y, Kang I-A, Don G-H, Yoon H-G, Park B-D and Wu Q. Thermal and mechanical properties of wood flour/talc-filled polylactic acid composites: effect of filler content and coupling treatment. *J Thermoplast Compos Mater* 2008; 21: 209–223.
12. Lin LH, Liu HJ and Yu NK. Morphology and thermal properties of poly(L-lactic acid)/organoclay nanocomposites. *J Appl Polym Sci* 2007; 106: 260–266.
13. Murariu M, Ferreira AD, Degee P, Alexandre M and Dubois P. Polylactide compositions. Part 1: effect of filler content and size on mechanical properties of PLA/calcium sulfate composites. *Polymer* 2007; 48: 2613–2618.
14. Paul MA, Alexander M, Degee P, Henris C, Rulmont A and Dubois P. New nanocomposite materials based on plasticized poly(L-lactide) and organo-modified montmorillonites: thermal and morphological study. *Polymer* 2003; 44: 443–450.
15. Pilla S, Gong S, O'Neill E, Rowell RM and Krzysik AM. Polylactide-pine wood flour composites. *Polym Eng Sci* 2008; 48: 578–587.
16. Pluta M, Jeszka JK and Boiteux G. Polylactide/montmorillonite nanocomposites: structure, dielectric, viscoelastic and thermal properties. *Eur Polym J* 2007; 43: 2819–2835.
17. Graupner N, Herrmann AS and Mussig J. Natural and man-made cellulose fibre-reinforced poly(lactic acid) (PLA) composites: an overview about mechanical characteristics and application areas. *Composites Part A* 2009; 40: 810–821.
18. Krishnamachari P, Zhang J, Lou JZ, Yan JZ and Uitenham L. Biodegradable poly(lactic acid)/clay nanocomposites by melt intercalation: a study of morphological, thermal, and mechanical properties. *Int J Polym Anal Charact* 2009; 14: 336–350.
19. Bledzki AK and Gassan J. Composites reinforced with cellulose based fibers. *Prog Polym Sci* 1999; 24: 221–274.
20. Wu CS and Liao HT. Modification of biodegradable polylactide by silica and wood flour through a sol-gel process. *J Appl Polym Sci* 2008; 109: 2128–2138.
21. Ogata N, Jimenez G, Kawai H and Ogihara T. Structure and thermal/mechanical properties of poly(l-lactide)-clay blend. *J Polym Sci Part B – Polym Phys* 1997; 35: 389–396.
22. Krikorian V and Pochan DJ. Poly(L-lactic acid)/layered silicate nanocomposite: fabrication, characterization, and properties. *Chem Mater* 2003; 15: 4317–4324.
23. Pluta M. Morphology and properties o polylactide modified by thermal treatment, filling with layered silicates and plasticization. *Polymer* 2004; 45: 8239–8251.
24. Ray SS, Maiti P, Okamot M, Yamada K and Ueda K. New polylactide/layered silicate nanocomposites. 1 preparation, characterization, and properties. *Macromolecules* 2002; 35: 3104–3110.
25. Ray SS, Okamoto K, Yamada K and Okamot M. Novel porous ceramic material via burning of polylactide/layered silicate nanocomposite. *Nano Lett* 2002; 2: 423–425.
26. Ray SS, Yamada K, Okamot M, Fujimoto Y, Ogami A and Ueda K. New polylactide/layered silicate nanocomposites. *5 designing of materials with desired properties*. Polym Compos 2003; 44: 6633–6646.
27. Ray SS, Yamada K, Okamot M, Ogami A and Ueda K. New polylactide/layered silicate nanocomposites. 3 high-performance biodegradable materials. *Chem Mater* 2003; 15: 1456–1465.
28. Ray SS, Yamada K, Okamot M, Ogami A and Ueda K. New polylactide/layered silicate nanocomposites. 4 structure, properties and biodegradability. *Compos Interfaces* 2003; 10: 435–450.
29. Ray SS, Yamada K, Okamot M and Ueda K. New polylactide-layered silicate nanocomposites. 2 concurrent

improvements of materials properties, biodegradability and melt rheology. *Polym Compos* 2003; 44: 857–866.
30. Ray SS, Yamada K, Okamoto M and Ueda K. Polylactide-layered silicate nanocomposite: a novel biodegradable material. *Nano Lett* 2002; 2: 1093–1096.
31. Shibata M, Someya Y, Orihara M and Miyoshi M. Thermal and mechanical properties of plasticized poly(L-lactide) nanocomposites with organo-modified montmorillonites. *J Appl Polym Sci* 2006; 99: 2594–2602.
32. Ludvik CN, Glenn GM, Klamczynski AP and Wood DF. Cellulose fiber/bentonite clay/biodegradable thermoplastic composites. *J Polym Environ* 2007; 15: 251–257.
33. Serna C, Ahlrichs JL and Serratosa JM. Folding in sepiolite crystals. *Clays Clay Miner* 1975; 23: 119–124.
34. Dinwoodie JM. *Wood: nature's cellular polymeric fiber-composite*. London: The Institute of Metals, 1989.
35. English BW and Falk RH. *Factors that affect the application of wood fiber-plastic composites*. Madison, WI: Forest Products Society, 1995.
36. Kazayawoko M and Balatinecz JJ. Surface modification and adhesion mechanisms in woodfiber-polypropylene composits. *J Mater Sci* 1999; 34: 6189–6199.
37. Cornelissen T, Yperman J, Reggers G, Schreurs S and Carleer R. Flash co-pyrolysis of biomass with polylactic acid. Part 1: Influence on bio-oil yield and heating value. *Fuel* 2008; 87: 1031–1041.
38. Paul MA, Delcourt C, Alexandre D, Degee P, Monteverde F and Dubois P. Polylactide/montmorillonite nanocomposites: study of the hydrolytic degradation. *Polym Degrad Stab* 2005; 87: 535–542.
39. Bandyopadhyay S, Chen R and Giannelis EP. Biodegradable organic-inorganic hybrids based on poly(L lactic acid). *Polym Mater Sci Eng* 1999; 81: 159–160.
40. Kopinke FD, Remmler M, Mackenzie K, Moder M and Wachsen O. Thermal decomposition of biodegradable polyesters-II. Poly(lactic acid). *Polym Degrad Stab* 1996; 53: 329–342.
41. Suming L. Hydrolytic degradation characteristics of aliphatic polyesters derived from lactic and glycolic acids. *J Biomed Mater Res* 1999; 48: 342–353.
42. Wang G and Li A. Thermal decomposition and kinetics of mixtures of polylactic acid and biomass during copyrolysis. *Chin J Chem Eng* 2008; 16: 929–933.